

Experimental generation of steering odd dark beams of finite length

A. Dreischuh, D. Neshev

*Sofia University, Department of Quantum Electronics, 5, J. Bourchier Blvd., BG-1164 Sofia, Bulgaria
(Fax.: +3592/9625276, E-mail: ald@phys.uni-sofia.bg)*

G. G. Paulus¹, H. Walther^{1,2}

¹*Max-Planck-Institut für Quantenoptik, Hans-Kopfermann-Straße 1, D-85748 Garching, Germany
(Fax.: +4989/329050, E-mail: ggp@mpq.mpg.de)*

²*Ludwig-Maximilians-Universität, Sektion Physik, Am Coulombwall 1, D-85747 Garching, Germany
(Fax.: +4989/2891 4142, E-mail: Prof.H.Walther@mpq.mpg.de)*

(October 29, 2018)

In this work we report the first realization of odd dark beams of finite length under controllable initial conditions. The mixed edge-screw phase dislocations are obtained by reproducing binary computer-generated holograms. Two effective ways to control the steering of the beams are analyzed experimentally and compared with numerical simulations.

OCIS code: 0190 4420; 0190 5940; 090 1760

I. INTRODUCTION

Physically, Dark Spatial Solitons (DSSs) are localized intensity dips existing on stable background beams as a result of an exact counterbalance of diffraction and nonlinearity. A necessary condition for their existence is the presence of a phase dislocation in the wavefront along which the phase is indeterminate and the field amplitude is zero. Besides the intriguing physical picture, the particular interest in the DSSs is motivated by their ability to induce gradient optical waveguides in bulk self-defocusing nonlinear media [1,2,3,4,5]. The only known truly two-dimensional (2D) DSSs are the Optical Vortex Solitons (OVSs) [2], whereas in one transverse spatial dimension DSSs manifest themselves as dark stripes [6]. The odd initial conditions required to generate a fundamental 1D DSS correspond to an abrupt π -phase jump centered along the irradiance minimum of the stripe. The OVSs have a more complicated phase profile described by $\exp(im\varphi)$, where φ is the azimuthal coordinate in a plane perpendicular to the background beam propagation direction and m – the so-called topological charge (TC) – is an integer number. This phase function ensures a π -phase jump in each diametrical slice through the vortex core. Fundamental DSSs of these types have the common feature of zero transverse velocity if no perturbations are present. In contrast to that, ring dark solitary waves [7] slowly change their parameters even when born from ideal odd initial conditions [8].

In the pioneering work of Nye and Berry [9] it is conjectured that mixed edge-screw dislocations cannot exist. Despite that, almost two decades later an indication for their existence was found [10] for two interacting optical vortices of opposite topological charges. In our recent experiments on the generation of quasi-2D DSSs [11] we found that moderate saturation of the nonlinearity can stabilize the snake instability which usually leads

to their decay. This made possible the first identification of 1D Odd Dark Beams (ODBs) of finite length with their characteristic edge-screw phase dislocations [11,12]. The mixed dislocation forces the dark beams to steer in space. This appears to be of practical interest [12] provided that there are effective ways to control the ODBs transverse velocity.

In this article we report the first experimental realization of steering odd dark beams of finite length with mixed phase dislocations under controllable initial conditions. Two approaches to control their transverse velocity are investigated experimentally and compared with numerical simulations.

II. EXPERIMENTAL SETUP AND RESULTS

A. Computer-generated holograms

The phase portrait of the mixed edge-screw dislocation (see Fig. 1 in Ref. [12]) consists of a pair of semi-helices with a phase difference of π to which an effective topological charge of $\pm 1/2$ can be ascribed. Their spatial offset $2b$ determines the length of the edge part of the dislocation and ensures a phase jump of $\Delta\varphi$ in the direction perpendicular to the dark stripe of finite length. The phase function of this mixed phase dislocation can be described by

$$\Phi_{\alpha,\beta}(x,y) = \Delta\varphi \left\{ -\frac{\beta}{\pi} \arctan\left(\frac{\alpha x}{y + b\beta}\right) + \frac{(1-\alpha)}{2} \text{sgn}(x) \right\}, \quad (2.1)$$

where x and y denote the transverse Cartesian coordinates perpendicular and parallel to the dark beam. $2b$ stands for the length of the edge part of the dislocation and

$$\alpha = \begin{cases} 0 & \text{for } |y| \leq b \\ 1 \text{ and } \beta = -1 & \text{for } y > b \\ 1 \text{ and } \beta = 1 & \text{for } y \leq -b \end{cases} . \quad (2.2)$$

The pattern of the Computer-Generated Holograms (CGHs) used to produce this phase distribution consists of parallel lines which become curved at the position of the semi-vortex cores. In the edge part of the dislocation they terminate and reappear shifted, for a π -jump by one half of the pattern period. Holograms with such structures correspond to interference lines shifted along an imaginary line of finite length and to curved lines limiting the dislocations as observed in our previous experiment (see Fig. 8 in [11]). The binary CGHs used are photolithographically fabricated with a grating period of $20\mu m$. Several holograms with various lengths of the edge part of the dislocation are etched on a common substrate. Special attention was paid to align the edge parts of the different dislocations correctly on their common substrate. The simplicity of varying the dislocation length and magnitude of the phase jump is the main advantage [13] of the approach we have chosen. The diffraction efficiency at first orders is measured to be 9%, close to the theoretical 10% limit for binary holograms. The unavoidable quantization inaccuracy of $\pi/24$ [14] for holograms of this type is negligible for measurements with phase jumps of $\Delta\varphi = 3\pi/4$, π , and $5\pi/4$ which are presented in this work.

B. Experimental setup

The setup used is similar to that in our previous experiments (see Fig. 1 in Ref. [11]). Briefly, the beam of a single-line Ar^+ laser ($\lambda = 488nm$) is used to reconstruct the CGHs. The first-diffraction-order beam with the phase dislocation nested in is filtered through a slit and is focused on the entrance of the $10cm$ long Nonlinear Medium (NLM). After the desired propagation path length, the beam is deflected by a prism immersed in the nonlinear liquid and is projected directly on a Charge-Coupled Device (CCD) camera array with a resolution of $13\mu m$. The NLM is ethylene glycol dyed with DODCI (Lambdachrome) to reach an absorption coefficient of $0.107cm^{-1}$. In a calibration measurement we generated 1D DSSs by using CGHs of the type described in Sec. I. The soliton constant Ia^2 (i.e. the product of the background-beam intensity I and the square of the dark beam width a measured at the $1/e$ -level) was found to reach its asymptotically constant value for input powers of $P_{sol}^{1D} \approx 33mW$. It is known that thermally self-defocusing liquids are both nonlocal and saturable. Since the saturation of the nonlinearity is able to modify the ODBs transverse velocity and profile, we needed to estimate it and to account for it in our numerical calculations. In an independent measurement we realized a self-bending scheme similar to that used in [15,16]. The asymmetry required was introduced by an intentional tilt

of the prism immersed in the NLM, which resulted in different nonlinear propagation path-lengths for the different parts of the background beam. The strength of the self-bending effect was measured in the near field. For an absorptive nonlocal medium the choice of a suitable saturation model is not trivial ([17], see also Sec. IV of [18]). We found a good fit for the experimental data with the equation $\Delta y \sim I/(1 + I/I_{sat})^\gamma$. Using it we estimated $P_{sat} \approx 100mW$ and $\gamma = 3$. In addition to the careful alignment of the CGHs on the substrate, the holograms were reproduced to achieve *vertical* dark beam steering, which is not sensitive to possible undesired weak horizontal self-deflection of the background beam. Changing the ODB parameters (length-to-width ratio and magnitude of the phase jump) was performed by a strict horizontal translation of the substrate. The accuracy of the alignment was tested by checking for equal steering of the ODBs reproduced from two identical holograms placed at opposite ends of the series of aligned CGHs. In this work the ODBs are identified by the corresponding lengths $2b$ of the edge portions of the dislocations in CGH pixels ($1pix. = 5\mu m$) as encoded in the holograms. The deflection Δx of the dark beams is measured in units of CCD camera pixels. We estimate that measurements with an encoded dislocation length of $b/5\mu m$ CGH pixels corresponds to a dislocation length-to-ODB width ratio ($2b/a$) = $1/10b/5\mu m$ in the numerical simulations (e.g. 14 pix. dislocation length corresponds to $b/a = 1.4$ in the simulations).

C. ODB steering vs. dislocation length

All data presented in this subsection refer to π phase jumps across the edge parts of the mixed dislocations. In Fig. 1a we plot the deflection Δx of ODBs with different dislocation lengths for input powers of $1.7mW$ (circles), $33mW$ (triangles) and $67mW$ (squares). The data obtained at $P = 1.7mW$ refer to a linear regime of propagation. The results at $33mW$ and $67mW$ are extracted from the experimental pictures shown in Fig. 1b and Fig. 1c, respectively, which are recorded for a nonlinear propagation path length of $z = 8.5cm$. The general tendency of linear increase of the deflection with decreasing the dislocation length is clearly expressed (Fig. 1a, solid line). The shortest mixed phase dislocation encoded was only $1pix.$ long. In this case the strong deviation from the linear dependence is caused by the annihilation of the semi-charges due to the shortening of the edge part of the dislocation. It will be shown later that this shortening accelerates for higher input powers (intensities). For that reason, even the ODB with an initially $10pix.$ long phase dislocation appears gradually less deflected at $P = 67mW$ as compared to the case of $P = 33mW$ (Fig. 1a). In Fig. 1b,c the thick solid lines are intended to denote the positions of the ODBs at the entrance of the NLM. Because ODB steering is present also in the

linear regime of propagation (Fig. 1a, dots) these positions (with respect to the dark beam intensity minimum and trailing peak maximum) are identified by numerical simulations for $b/a = 2.5$. The identification corresponds to an encoded dislocation length of $25pix.$, i.e. to the most right frame shown in Fig. 1b,c. Somewhat surprising is the weak sensitivity of the ODB deflection vs. background beam power (intensity) far from TC annihilation. It can be intuitively understood by recalling the known interaction scenario of well-separated OVSs of opposite TCs [19,20]. In this case the attraction between the OVSs is negligible as compared to their translation as a pair. At a constant input power of $33mW$ we measured the ODB deflection vs. nonlinear propagation path length (Fig. 2). As expected, the ODB with $10pix.$ long dislocation has higher transverse velocity than that one with $22pix.$ long dislocation. The linearity in the dependencies is also well pronounced.

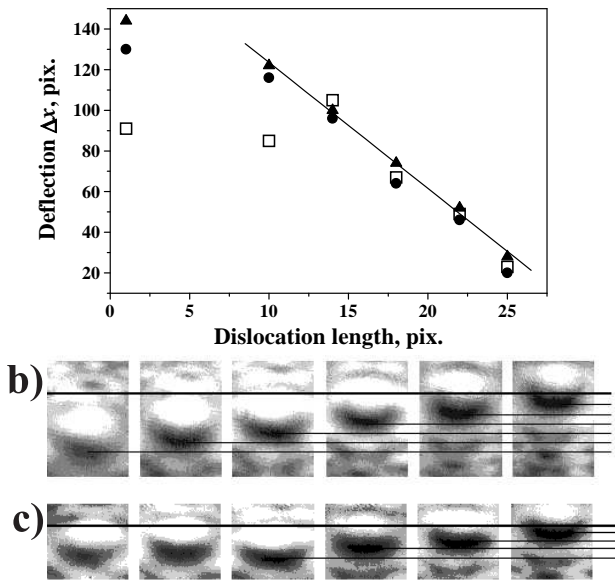


FIG. 1. Deflection of odd dark beams of finite length vs. dislocation length at input powers of $1.7mW$ (dots), $33mW$ (triangles), and $67mW$ (squares) for $z = 8.5cm$ and $\Delta\varphi = \pi$ (a). The points are extracted from the frames shown in Fig.1b ($33mW$) and Fig.1c ($67mW$). From left to right the frames correspond to $b = 1, 10, 14, 18, 22,$ and $25pix.$, respectively. The thick solid line indicates the calculated position of the ODB at the entrance of the NLM for $b = 25pix.$.

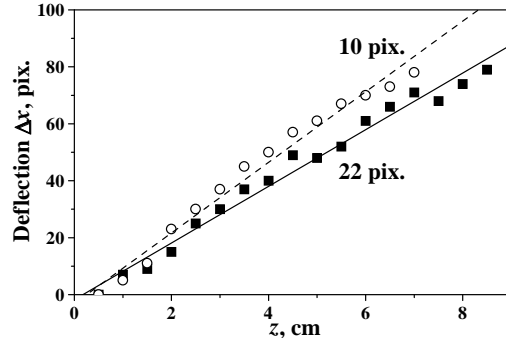


FIG. 2. Deflection Δx vs. nonlinear propagation path length z for encoded dislocation lengths of $10pix.$ (circles) and $22pix.$ (squares). The dashed and the solid lines are the respective linear fits. ($P = 33mW$; $\Delta\varphi = \pi$).

D. Phase control of the ODB steering

As a second possible way to control the dark beam deflection, we considered the variations in the magnitude of the phase jump $\Delta\varphi$ across the edge part of the mixed dislocation. In Fig. 3 we compare the experimental dependencies $\Delta x(\Delta\varphi) |_{b=22pix.}$ (squares) and $\Delta x(b) |_{\Delta\varphi=\pi}$ (dots). The straight lines are the respective linear fits. Because a problem in encoding a larger set of phase jumps in the CGHs was recognized too late, we measured the deflection Δx at $\Delta\varphi = 3\pi/4, \pi,$ and $5\pi/4$ only. In view of that the linear fit of the phase dependence in Fig. 3 appears to be assailable. Its linearity, however, is confirmed by numerical simulations (see Sec. III). The dependence of Δx on $\Delta x(\Delta\varphi)$ and $\Delta x(b)$ has been plotted in one figure in order to underline the fact that it appears to be easier to deflect the ODB by controlling the phase than by controlling the dislocation length. The measurements are performed at a constant power of $33mW$.

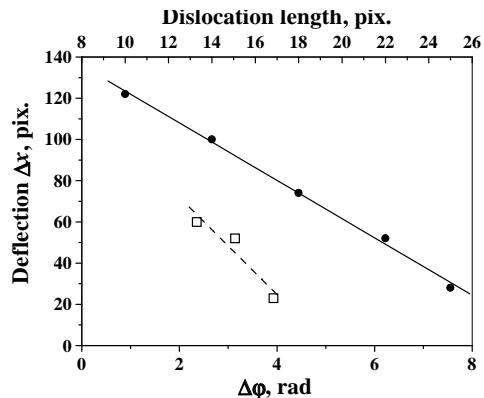


FIG. 3. ODB deflection vs. magnitude of the phase jump $\Delta\varphi$ (hollow squares) and the dislocation length as encoded in the CGHs (dots). The straight lines are linear fits. ($P = 33mW$).

E. Power/Intensity dependencies

The ability of the dark spatial solitons [2,3,4,5] (and the dark spatial waves [21,22]) to induce gradient all-optical waveguides in bulk self-defocusing NLM originates in the negative nonlinear correction to the linear refractive indices of the media. In view of that, the intensity dependencies remain undoubtedly of interest, despite of the low sensitivity of the ODB steering on the input power (intensity). In Fig. 4 we present experimental data on the power dependence of the length of the edge portion of the mixed dislocation for $\Delta\varphi = \pi$ and for two different lengths of $14pix.$ and $22pix.$ encoded in the holograms. It is easy to understand that the (mixed) phase dislocations do not remain sharp and of an unchanged magnitude when the (odd) dark beam steers [23]. The dislocation lengths are estimated by evaluating the respective longitudinal ODB slices at 5% of the background beam intensity (i.e. at the actual noise level in the recorded frames). Generally, the dislocation length decreases monotonically with increasing the input power. Asymptotically, the dislocation flattens and disappears, provided that the ratio b/a is less than 2. As mentioned in [12], at $b/a \sim 4$ the ODBs should be expected to bend due to the snake instability [17]. In fact we observed such a behavior for ODBs with encoded dislocation lengths ranging from 4 to 6. A vortex-beam creation is recognized by the convergence of two neighboring interference lines in one. However, the vortices formed by this instability remained with highly overlapping cores [17,24].

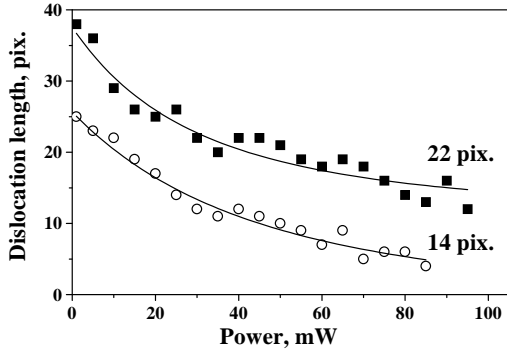


FIG. 4. Edge dislocation length vs. input background beam power for two different dislocation lengths encoded in the CGHs. ($\Delta\varphi = \pi$; $z = 8.5cm$)

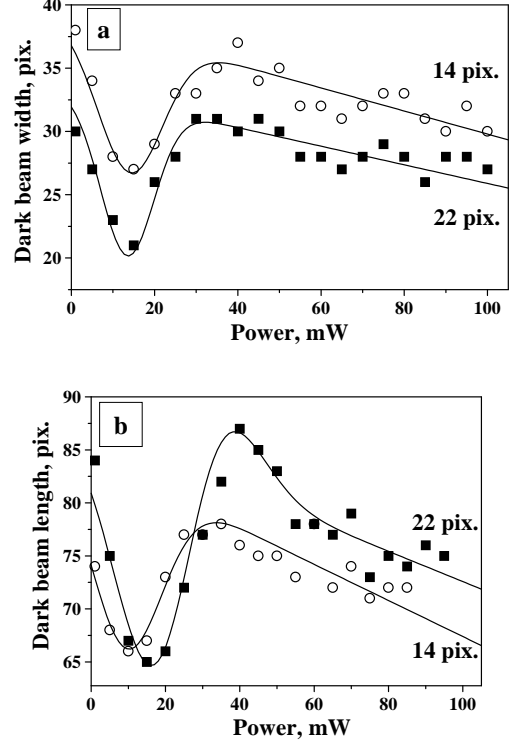


FIG. 5. ODB width (a) and length (b) (at the $1/e$ level) vs. input background-beam power for two different dislocation lengths encoded in the CGHs. ($z = 8.5cm$)

In Fig. 5a,b we plot the measured ODB widths (a) and their lengths (b) at the $1/e$ -level as a function of the background beam power. The initial lengths of the mixed phase dislocations are denoted in pixels as encoded on the respective CGHs, whereas the widths and lengths at the exit of the NLM are measured in units of CCD camera pixels. The strong decrease in both the ODB width and length up to $17mW$ (approximately $P_{sol}^{1D}/2$) is followed by an approximate recovering of the width and length at approximately P_{sol}^{1D} . At higher input powers both transverse quantities decrease but the tendency is slower as compared to the situation below $P_{sol}^{1D}/2$ and stabilizes asymptotically at high saturation. As it will be discussed in the next section, the minima in the curves plotted in Fig. 5a,b result from the reshaping of the OD beams at the particular $1/e$ intensity-level chosen for evaluation. The estimation there shows that the first rapid decrease in both transverse dimensions of the ODBs does not correspond to a ‘soliton constant’ formation. Generally speaking, the ODBs analyzed are no solitary waves in the widely adopted sense, since they do not survive, for instance, a collision with a second ODB steering in the opposite direction [12]. Nevertheless, the narrowing in both transverse directions for higher powers (intensities) should improve their guiding ability when signal beams or pulses are to be transmitted inside the ODBs and deflected in space. This feature will be addressed elsewhere. It is interesting to note that, independent of the length

of the mixed dislocations (2b), the widths (a) of the dislocations should be initially equal (in the near field behind the CGHs), but appeared different near the entrance of the NLM. The estimation has shown a CGH-to-NLM distance of approximately 4 Rayleigh diffraction lengths with respect to the initial ODB width. The well pronounced separation between the curves in Fig. 5a should be attributed to the different two-dimensional diffraction at different initial ODB length-to-width ratios.

III. NUMERICAL SIMULATIONS

In our numerical simulations we tried to model the experimentally obtained dependencies by accounting for the estimated moderate saturation of the nonlinearity ($P_{sol}^{1D} = 33mW$; $P_{sat} = 100mW$ at $\gamma = 3$; see Sec. II B). The (2 + 1)-dimensional nonlinear evolution of the steering ODB of finite length in the bulk homogeneous and isotropic NLM is described by the generalized nonlinear Schrödinger equation

$$i \frac{\partial E}{\partial \zeta} + \frac{1}{2} \left(\frac{\partial^2}{\partial \xi^2} + \frac{\partial^2}{\partial \eta^2} \right) E - \frac{L_{Diff}}{L_{NL}} \frac{|E|^2}{(1 + s|E|^2)^\gamma} E = 0, \quad (3.1)$$

where the transverse spatial coordinates are normalized to the initial dark-beam width ($\zeta = x/a, \eta = y/a$), and the propagation path length is expressed in Rayleigh diffraction lengths $L_{Diff} = ka^2$. Further, $L_{NL} = (kn_2 I_0)^{-1}$ is the nonlinear length, k is the wavenumber inside the NLM, and I_0 is the background beam intensity. The adopted correction for the nonlinear refractive index is

$$\Delta n = n_2 |E|^2 / (1 + s|E|^2)^\gamma, \quad (3.2)$$

with $s = P_{sol}^{1D} / P_{sat} = 0.3$. As it was done in [12], the slowly varying electric-field amplitude of the ODB was chosen *tanh*-shaped

$$E(x, y) = \sqrt{I_0} B(r_{1,0}(x, y)) \tanh \left[\frac{r_{\alpha,\beta}(x, y)}{a} \right] e^{i\Phi_{\alpha,\beta}(x, y)}, \quad (3.3)$$

where $r_{\alpha,\beta}(x, y) = \sqrt{x^2 + \alpha(y + \beta b)^2}$ is the effective Cartesian/radial coordinate, $\Phi_{\alpha,\beta}$ is the phase distribution of the mixed edge-screw dislocation (see Eq. 2.1), and α and β are given by Eq. 2.2. The width w of the super-Gaussian background beam

$$B(r) = \exp \left\{ - \left(\sqrt{\frac{x^2 + y^2}{w^2}} \right)^{14} \right\} \quad (3.4)$$

is chosen to exceed at least 15 times the ODB lengths. The model equation (3.1) was solved numerically by the beam propagation method on a 1024×1024 grid. It

should be mentioned, that the initial width $a(z = 0)$ of the ODB of finite length was chosen to correspond to that of an infinite 1D ODSS ($a = a_{sol}^{1D} = const. I_0^{-1/2}$). It was proven numerically that the ODB deflection is insensitive to the particular value of a , and Figs. 6-8 are generated under this assumption. Actually, the nonlinearity causes an appreciable reshaping of the beams, in particular in the first evolution stage when the ODB starts steering, see Fig. 2 in Ref. [12]). In order to improve the similarity between the experimental data (Figs. 4 and 5) and the numerical results (Figs. 9 and 10), an initial ODB width twice as large as in the experiment is assumed. In Fig. 6 we plot the ODB deflection vs. $b/a|_{z=0}$ for different input powers (intensities). All data presented in this section refer to a normalized propagation path length of $z = 4L_{NL}$, which corresponds to that estimated for the experiment. Nevertheless all calculations are carried out up to $10L_{NL}$ whereby no qualitative deviation from the tendencies discussed is seen. The linearity in the ODB deflection vs. b/a is well obeyed except for $b/a > 2.2$. The longer ODBs steer slower, bend slightly, and decay into pairs of vortex beams for $b/a > 4$. In the linear regime of propagation, the ODBs also deflect but the deflection is stronger at higher input powers/intensities. This is more pronounced for shorter dislocations. In the experimental data (Fig. 1a), this behavior is much weaker, rather the deflection remains within the experimental accuracy. Looking for an adequate explanation, in a series of simulations we checked that a $\pm 30\%$ inaccuracy in estimating P_{sat} results only in $\pm 5\%$ deviation in the ODB deflection at $z = 4L_{NL}$. The observed tendency of a decrease of the ODB steering velocities at increased saturation is well understood [25] but seems insufficient in quantity. We attribute the absence of a well expressed power dependence in Fig. 1a to the NLM nonlocality. In a separate experiment it was estimated, that the nonlocality in this medium is negligible on a spatial scale of several hundred of micrometers only [18].

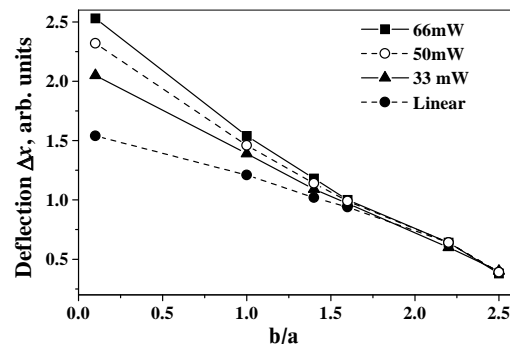


FIG. 6. Calculated ODB steering vs. b/a for different input powers with $\Delta\varphi = \pi$.

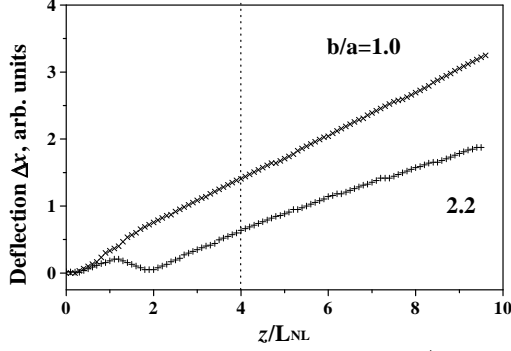


FIG. 7. ODB steering along the NLM for $b/a = 1.0$ and 2.2 . Crosses - some 10% of the numerical data. Vertical dashed line - propagation distance $z/L_{NL} = 4$ corresponding to the experimental conditions at $33mW$.

In Fig. 7 we plot the ODB deflection vs. the nonlinear propagation path length z/L_{NL} for $b/a = 1.0$ and 2.2 . As in the previous figure the magnitude of the edge part of the phase dislocation is set to $\Delta\varphi = \pi$. Once the ODB starts steering, its transverse velocity remains constant (see Fig. 2). The longer ODBs with longer edge dislocations, however, emit dispersive waves in their first evolution stage ($z < L_{NL}$). This causes a ‘delay’ in the steering along the NLM (Fig. 7, lower curve).

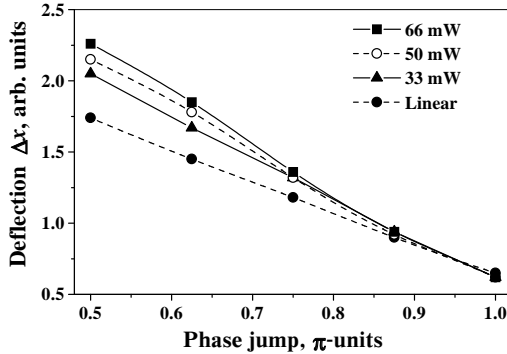


FIG. 8. Deflection of ODBs vs. phase jump $\Delta\varphi$ for $b/a = 2.2$ and for different input powers.

In Fig. 8 we present results obtained for the phase-dependent control of the ODB deflection at different input powers (intensities). In qualitative agreement with the experimental observation, the linear increase in the ODB steering with decreasing the magnitude of the phase jump down to $\Delta\varphi = 0.5\pi$ is evident. The comparison of Figs. 6 and 8 confirms the conclusion that at a fixed nonlinear propagation distance the phase-controlled ODB deflection is more efficient as compared to that by varying the b/a ratio.

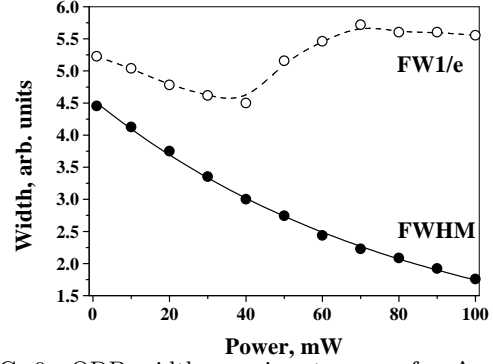


FIG. 9. ODB width vs. input power for $\Delta\varphi = \pi$ and $b/a = 1.4$. (Dashed curve: full width at the $1/e$ -intensity level; solid: FWHM).

Fig. 9 is intended to clarify the origin of the non-monotonic power dependencies of the ODB widths (and lengths) observed at input powers below P_{sol}^{1D} (see Fig. 5). The solid line represents the ODB full width at half maximum (FWHM), the dashed one the full width at the $1/e$ -intensity level. In these simulations $\Delta\varphi = \pi$ and $b/a = 1.4$ are assumed. Qualitatively, we obtained the same curves also for $b/a = 2.2$ by accounting for the initial free-space propagation in the experiment (from the CGH to the entrance of the NLM; $z \approx 4L_{Diff}$). The minimum in the ODB width evaluated at the $1/e$ level originates from the reshaping of the beam profile which is caused by the moderate saturation. A similar reshaping is reported in [26] (see Figs. 2-4 therein). At $b/a = 2.2$ the data obtained for the ODB length vs. input power (intensity) were found to be even more sensitive to the intensity level of evaluation. Because of the transverse steering of the ODBs of finite length the edge portions of the dislocations shorten monotonically with increasing the background beam power (intensity) (Fig. 10). The numerical results are in a very good qualitative agreement with the experimental ones (Fig. 4).

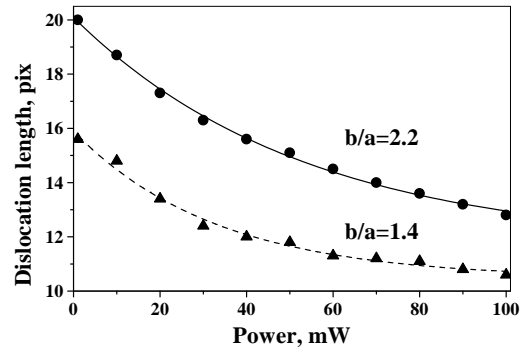


FIG. 10. Length of the edge portion of the mixed phase dislocation vs. input power for $\Delta\varphi|_{z=0} = \pi$ and $b/a = 1.4$ and 2.2 , respectively.

IV. CONCLUSION

The results presented show that the inherent steering dynamics of odd dark beams of finite length can be effectively controlled by varying both the magnitude $\Delta\varphi$ and the relative length b/a of the mixed edge-screw phase dislocation. The background-beam intensity has weak influence on the steering but is important for keeping the optically-induced gradient waveguides steep, which is crucial for all-optical guiding, deflection and switching of signal beams or pulses. Since the mixed phase dislocations shorten and flatten along the nonlinear media (tending asymptotically to washout) the ODBs seem to be promising primarily for future short-range all-optical switching devices.

ACKNOWLEDGMENTS

A. D. would like to thank the Alexander von Humboldt Foundation for the award of a fellowship and the opportunity to work in the stimulating atmosphere of the Max-Planck-Institut für Quantenoptik (Garching, Germany). This work was also supported by the National Science Foundation of Bulgaria.

-
- [1] Yu. S. Kivshar, B. Luther-Davies, *Physics Reports* **289**, 81 (1997).
 - [2] G. Swartzlander, Jr., C. Law, *Phys. Rev. Lett.* **69**, 2503 (1992).
 - [3] E. A. Ostrovskaya, Yu. S. Kivshar, *Opt. Lett.* **23**, 1268 (1998).
 - [4] A.H. Carlsson, J.N. Malmberg, E.A. Ostrovskaya, T.J. Alexander, D. Anderson, M. Lisak, and Yu. Kivshar, *lanl, patt-sol/9909009*, 30 Sept. (1999).
 - [5] C.T. Law, X. Zhang, and G.A. Swartzlander, *Opt. Lett.* **25**, 55 (2000).
 - [6] G. Allan, S. Skiner, D. Andersen, A. Smirl, *Opt. Lett.* **16**, 156 (1991).
 - [7] Yu. S. Kivshar, X. Yang, *Phys. Rev.* **E 50**, R40-R43 (1994); *ibid.* *Chaos, Solitons & Fractals* **4**, 1745 (1994).
 - [8] D. Neshev, A. Dreischuh, V. Kamenov, I. Stefanov, S. Dinev, W. Fließner, L. Windholz, *Appl. Phys.* **B 64**, 429 (1997).
 - [9] J. F. Nye, M. V. Berry, *Proc. R. Soc. London A* **336**, 165 (1974).
 - [10] V. Bazhenov, M. Soskin, M. Vasnetsov, *J. Mod. Opt.* **39**, 985 (1992); I. Basistiy, V. Bazhenov, M. Soskin, M. Vasnetsov, *Opt. Commun.* **103**, 422 (1993).
 - [11] A. Dreischuh, G. G. Paulus, F. Zacher, *Appl. Phys.* **B 69**, 113 (1999).
 - [12] A. Dreischuh, G. G. Paulus, F. Zacher, I. Velchev, *Appl. Phys.* **B 69**, 107 (1999).
 - [13] N. R. Heckenberg, R. McDuff, C. P. Smith, A. G. White, *Opt. Lett.* **17**, 221 (1992).
 - [14] W. -H. Lee, *Prog. Optics* **XVI**, 119 (1978).
 - [15] A. E. Kaplan, *JETP Lett.* **9**, 33 (1969).
 - [16] M. S. Bordin, A. M. Kamuz, *JETP Lett.* **9**, 351 (1969).
 - [17] V. Tikhonenko, J. Christou, B. Luther-Davies, Yu. S. Kivshar, *Opt. Lett.* **21**, 1129 (1996).
 - [18] A. Dreischuh, G. G. Paulus, F. Zacher, F. Grasbon, H. Walther, *Phys. Rev.* **E60**, 6111 (1999).
 - [19] K. Staliunas, *Chaos, Solitons & Fractals* **4**, 1783 (1994).
 - [20] D. Neshev, A. Dreischuh, M. Assa, S. Dinev, *Opt. Commun.* **151**, 413 (1998).
 - [21] A. Dreischuh, V. Kamenov, S. Dinev, *Appl. Phys.* **B 63**, 145 (1996).
 - [22] D. Neshev, A. Dreischuh, S. Dinev, L. Windholz, *J. Opt. Soc. Am.* **B 14**, 2869 (1997).
 - [23] R. Thurston, A. Weiner, *J. Opt. Soc. Am.* **B 8**, 471 (1991).
 - [24] A.V. Mamaev, M. Saffman, A. A. Zozulya, *Phys. Rev. Lett.* **76**, 2262 (1996).
 - [25] W. Krolikowski, N. Akhmediev, B. Luther-Davies, *Phys. Rev.* **E 48**, 3980 (1993).
 - [26] V. Tikhonenko, Yu. S. Kivshar, V. Steblina, A. Zozulya, *J. Opt. Soc. Am.* **B 15**, 79 (1998).